Colegio de Postgraduados

Effects of Groundwater Extractions and Agricultural Irrigation Through Spatial Analysis, Endorheic Watershed Case

Gutierrez-Montenegro, M. O.[1]; **Escobar-Flores, J. D.**[1]; **Sánchez-Ortiz, E.***

[1] Instituto Politécnico Nacional-Centro Interdisciplinario de Investigación para el Desarrollo Integral Regional Unidad Durango, IPN. Sigma 119, 20 de Noviembre II, C.P. 34220. Durango, Dgo. México.
* Correspondence: esanchezo@ipn.mx

ABSTRACT

Objective: To examine the relationship between human activity and the occurrence of ground fissures in Mennonite agricultural soils within the Laguna de Santiaguillo endorheic watershed.

Design/methodology/approach: Earth fissures were geolocated and digitized using satellite imagery. Remote sensing techniques were utilized to calculate the Normal Difference Moisture Index (NDMI) during the 2023-2024 agricultural cycles. Kernel density per Km^2 was calculated by concession and annual concessioned volume. Moreover, the total of rainfall in the study area was calculated using Thiessen polygons to be compared with the monthly NDMI.

Results: The study area has groundwater extractions throughout the year to meet the needs of hydric crops, which is observed through annual concession volume with an average density of 6.46 wells/Km^2. While the NDMI value for the agriculture cycle 2023 presents important variations in specific areas that zones containing major moisture are agricultural production areas, making it evident that the moisture patron is strongly related to agricultural activities in parcels that have a groundwater concession.

Limitations on study/implications: The study area presents significant pressure related to groundwater concessions. According to the Kernel analysis density, it was detected that one of the regions with major volume concessioned density coincides with one of the earth fissures detected through spatial images. These results suggest that this zone presents an advanced subsidence phenomenon. Kernel's density analysis was calculated based on the volume of CONAGUA's groundwater concessioned values; it is unknown the exact amount of groundwater extraction from the aquifer.

Findings/conclusions: One of the principal earth fissures coincides with a high Kernel's density estimation per annual volume concessioned, 30% of the total aquifer's concessions are in the study area, showing a high concentration of groundwater extractions.

Keywords: Aquifer, Earth Fissures, GIS Kernel's Density.

Citation: Gutierrez-Montenegro, M.O., Escobar-Flores J.D., & Sánchez-Ortiz, E. (2026). Effects of Groundwater Extractions and Agricultural Irrigation Through Spatial Analysis, Endorheic Watershed Case. Agro Productividad. https://doi.org/10.32854/2139k173

Academic Editor: Jorge Cadena Iñiguez
Associate Editor: Dra. Lucero del Mar Ruiz Posadas
Guest Editor: Juan Francisco Aguirre Medina

Received: September 26, 2025.
Accepted: December 16, 2025.
Published on-line: March 31, 2026.

Agro Productividad, 19(1). January. 2026. pp: 201-216.

INTRODUCTION

Groundwater accounts for 98% of the world's freshwater and is crucial to ecosystems, human consumption, industry, and particularly to agricultural irrigation in arid and semiarid regions (Barati *et al.*, 2019; Yan *et al.*, 2025).

Groundwater availability in several aquifers worldwide is decreasing, influenced by a combination of natural factors, including precipitation, slope, and lithology, as well as anthropogenic influences such as the number of wells, urbanization, industry, and agriculture. This phenomenon affects future food production (Redwan and Abdel Moneim, 2016; Whittemore *et al.*, 2023).

If the total of groundwater extracted over many years is close to or exceeds the total recharge, it's considered that there is overexploitation. In other words, an overexploited aquifer is defined as the amount of water extracted being greater than the volume that infiltrates. This term becomes more significant in arid or semi-arid areas due to the limited recharge capacity (Van Camp *et al.*, 2010).

In Mexico, 77% of the volume of water extracted is used for the agricultural sector. However, there are three significant constraints on this use: a) Seasonal distribution of rainfall over four months of the year (June- September) with the rest of the year relatively dry; b) Distribution of rainfall across the country, states like Tabasco (southeast) rainfall is close to 2,095 mm per year, while Baja California Sur (northwest) only 160 mm is received; c) in the northern, central and northwestern regions of the country natural water availability is 31%, and with 77% of total population living there, it generates 87% of GDP. These three limitations result in a heavy dependence on groundwater for agricultural activities, leading to overexploitation of more than 100 aquifers in the country. This lowers water tables, resulting in settlements and landslides (SEMARNAT, 2010).

Agriculture is the primary water consumer worldwide, utilizing approximately 72% of the world's renewable water resources. Its expansion has increased water demand, leading to excessive groundwater extraction and subsidence phenomena. This may trigger earth fissures that affect the surrounding communities' infrastructure, as well as permanently affect aquifer compaction and decrease storage capacity (Fan *et al.*, 2025; Song *et al.*, 2023).

Subsidence is a phenomenon that has been present in recent years. This is a superficial manifestation of overexploitation of natural resources (hydrocarbons, vapor, minerals, or groundwater) that changes the state of soil efforts (Alvarez *et al.*, 2001).

Intensive groundwater extraction reduces pore pressure in granular media, causing land deformation and compaction of unconsolidated sediments (Solano Rojas *et al.*, 2015). When groundwater extraction is greater than recharge, cones of abatement are formed, and it's associated with three deformation stages 1) sinking for water abatement; 2) fissure generation, and 3) fissure growth. Figueroa-Miranda *et al.* (2018) define an Earth fissure as any discontinuity related to subsidence caused by groundwater extraction in alluvial or lacustrine valleys.

The Earth fissure formation process is complex; they are characterized by soil and superficial rock breakage resulting from a combination of various natural geographic phenomena, as well as human activities. Among the leading causes are geological structures and soil sinking from groundwater extraction. Superficial water runoff process and erosion contribute to fissure development, increasing the weight and length of small fissures located under the surface. These superficial processes could be increased fissure impacts, creating severe damage (Jia *et al.*, 2021; Li *et al.*, 2024).

The use of special tools eases the processes, the results of which can be geographically analyzed. Creation of Kernel density maps enables the identification of major pressure areas, either for point concentration or any specific value or attribute of interest (Díaz Caravantes *et al.*, 2013).

During the decade 2010-2020, remote sensors were used to make temporal and spatial monitoring of the superficial hydrological resources' variations and drought in different parts of the world. These methods allowed to get parameters such as Normalized Differential Water Index (NDWI), Normalized Differential Vegetation Index (NDVI), Normalized Differential Moisture Index (NDMI), and Soil-adjusted Vegetation Index (SAVI) (Song *et al.*, 2025; Tibangayuka *et al.*, 2025).

Some research shows that subsidence in agricultural areas is related to hydric resources management in cases where excessive water use might increase land subsidence, directly impacting agricultural productivity (Guzy and Malinowska, 2020).

Territory management keeps a significant relationship with subsidence phenomena, which is why it is essential to analyze how agricultural practices affect these processes (Minderhoud *et al.*, 2018).

Inside Mennonite agricultural areas located in the Laguna de Santiaguillo watershed, Durango, México, fissures related to subsidence processes have been observed. These fissures present a relatively limited extension and a lack of visible soil mass movements, and they are scattered and non-patterned. However, due to the impact that is generated in the agricultural landscape and the region's productive activities, their study results are relevant to this research.

Given the limitations of the use of interferometry techniques described above and the need to establish management planning criteria to prevent significant risk effects, this study proposes to use indicators that integrate the leading causes and subsidence effects.

This study examines the relationship between human activities and the occurrence of earth fissures in Mennonite agricultural soils within Laguna de Santiaguillo watershed, Durango, Mexico, employing a geospatial approach that incorporates territorial management indicators, resources, and soil conditions.

MATERIALS AND METHODS

The research was conducted in Laguna de Santiaguillo endorreic watershed, located in the north-center of Durango State, Mexico, within hydrologic region number 11, north of the San Pedro-Mezquital River. Hydrologic net flows to two lagoons, which are also important migratory bird routes in North America, support about 67 species that reside there in winter, some of them coming from Alaska and Canada. Laguna de Santiaguillo is recognized as an Area of Importance for Bird Conservation (AICA, in Spanish) and was declared a Ramsar site in 2012 (Cassio Madrazo and Sánchez Ortiz, 2018; Corral-Bermudez *et al.*, 2019).

In the 1920s, a series of Mennonite communities' settlements were established in the area. Since their arrival until the present day, the principal economic activities undertaken by the population have been agriculture and cattle raising (Hansen, 2005).

The study area spans 167.9 ha and encompasses the Mennonite communities of the region. Geographically, it is located within extreme coordinates: W −105.07°, S 24.83°, E −104.93°, and N 25.02° (Figure 4).

According to INEGI information, the topoform system comprises an alluvial plain (162.286 ha) and a floodable alluvial plain (5.04 ha). Its climate is semi-dry temperate, with summer rain (BS1kw(w)), and Vertisol is the predominant edaphology.

Mexican Geological Service (SGM) reports that the study area presents a stratigraphy from the Cenozoic, Quaternary period with alluvial sediments (sand and lime) and lacustrine (clays). Geological faults are not reported in the study area; the nearest are Chapala and Morillitos faults located 12 and 11 Km away, respectively. These faults are classified as normal faults provoked by superficial tension that trigger an inclined vertical slide of 60° (Figure 4).

Kernel density analysis

Based on Díaz Caravantes *et al*., (2013) methodology and using ArGis 10-8 an analysis of Kernel density was made, using a cell size of 30×30 m (Figure 8 and 9), whose principle is the continuous surfaces construction from points, in this case were used the wells distributed in the zone, as well as an analysis including the annual quantity of concessioned volume per REPDA concession, this represented areas of water use density and classified as high, medium and low enabling to establish areas where is concentrated a central pressure per Km^2 to aquifer.

To estimate the calculation of surfaces, the Kernel method uses the calculation of density observations around a pixel (Equation 1). The Kernel's quadratic function used in ArcGIS is:

$$D_{(s)} = \sum_{i=1}^{n} Si\left(3 / \pi\tau^2\right)\left[1-\left(h_i^2 / \tau^2\right)\right]^2 \quad (1)$$

Where τ is the radius of the circles of nearby points, h_i is the distance between point s and the observed point S_i, n is the number of observed points, and $D_{(s)}$ is the density on that point.

The results achieved allow the creation of maps that spatially distribute areas with greater pressure on the aquifer. In this research, a radius of 569.14 m was delimited to get an influence area of 1 Km^2.

Given that the results do not have a normal distribution, they were reclassified by Jenks' natural breaks method. This reclassification creates classes where similar values cluster more effectively and increases the difference between classes. In this manner, entities are divided into classes, for which limits are established where considerable differences exist between values and data. A blue-yellow-red color ramp was utilized to represent high, medium, and low-density zones. Blue represents low-density zones, yellow represents medium, and red represents high-density zones.

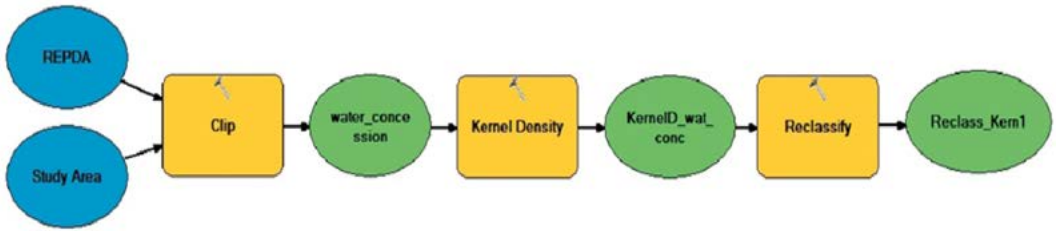

Figure 1. Work diagram to estimate the Kernel's density per Km^2. Blue ovals indicate that users only have to load the spectral bands of their interest. Yellow squares are geospatial processes, and green ovals are the result of each geoprocess.

Normalized differential moisture index (NDMI)

Monthly multispectral imagery from March 2023 to March 2024 was downloaded from the U.S. Geological Survey (USGS) http://glovis.usgs.gov/ from the Operation Land Imager (OLI) Landsat 8 and 9 collection 2 level 2 instrument, Path 31, Row 43, and cloud cover less than 30%.

To calculate NDMI, the Bo-Cai Gao (1996) technique was employed, utilizing remote sensors to estimate the moisture content in vegetation, through two narrow channels located at 0.86 μm and 1.24 μm wavelengths (Equation 2). The results obtained are from −1 to 1, describing the crops' hydric stress levels (Table 1).

NDMI is calculated by the quotient of the difference between and the sum of radiation reflected within the near infrared region band (NIR) and the shortwave infrared region, using the equation:

$$NDMI = \frac{NIR - SWIR}{NIR + SWIR} \quad (2)$$

For Landsat 8 and 9 S2 L2 images NIR band corresponds to band 5 and SWIR band corresponds to band 6 (Equation 3)

$$NDMI = \frac{Band\,5 - Band\,6}{Band\,5 + Band\,6} \quad (3)$$

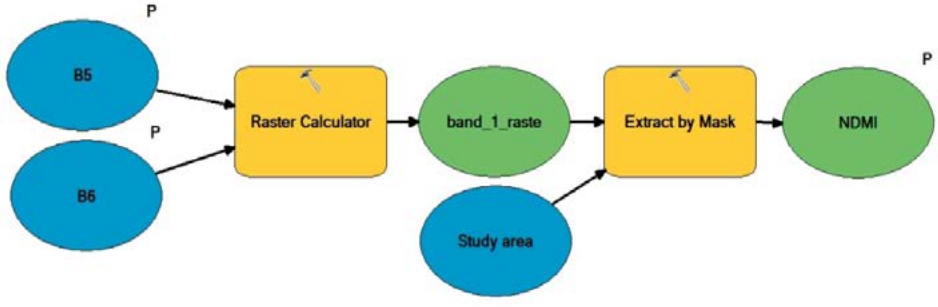

Figure 2. ArcGIS method to calculate NDMI. Blue ovals have a P superscript indicating that users only have to load spectral bands of their interest. Yellow squares are geospatial processes, and green ovals are the result of each geoprocess.

Table 1. Parameters of interpretation of NDMI results.

Value	Interpretation
−1 - −0.8	Bare ground
−0.8 - −0.6	Almost non-existent canopy cover
−0.6 - −0.4	Very low canopy cover
−0.4 - −0.2	Low and dry canopy cover
−0.2 - 0	Medium-low canopy cover and high-water stress
0 - 0.2	Medium canopy cover and high-water stress
0.2 - 0.4	Medium-high canopy cover and high-water stress
0.4 - 0.6	High canopy cover, no water stress
0.6 - 0.8	Very high canopy cover, no water stress
0.8 - 1	Full canopy cover, no water stress/flooding

Calculating this index allows the analysis of soil moisture or hydric stress periods in regional crops. Using this index, the irrigation time and its intensity could be estimated during rainless periods, as well as in extreme or abnormal drought conditions.

Precipitation analysis

National Meteorological Service (SMN) (Servicio Meteorológico Nacional, in Spanish) is the government agency responsible for recording and providing weather information to the national and local level of Mexican Republic, SMN constantly monitors atmospheric variables through 2,400 active meteorological stations distributed throughout the country and has a monthly database rainfall from meteorological station, in this study the information was taken from Tejamen station (10083), Guatimapé station (10137) and Coneto de Comonfort station (10129), using ArcGIS 10.8 algorithms, Thiessen polygons were created to establish the regionalization of rainfall in the study area (Figure 3), the area of influence of each station was calculated and multiplied by the monthly precipitation data, with this information, histograms were created to know the trend of rainfall in the area and identify extreme drought phenomena in the region.

Using a comparative analysis of precipitate volume and NDMI corresponding to the agricultural cycle 2023 was possible to visualize anthropogenic influence on the humidity of the study area caused by periods of low water and drought.

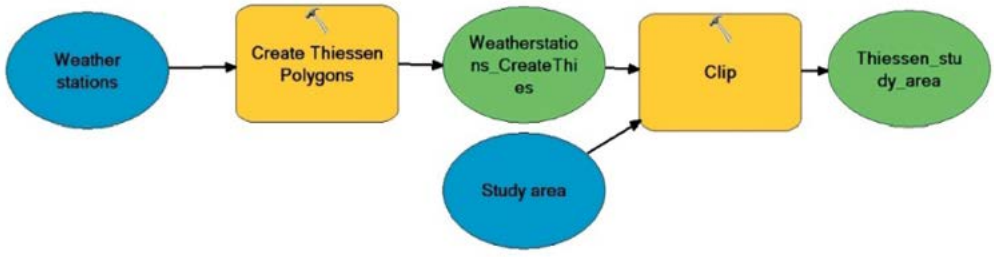

Figure 3. Method utilized to calculate precipitate volume in the study area. Blue ovals indicate that users only have to load the spectral bands of their site of interest. Yellow squares are geospatial processes, and green ovals are the result of each geoprocess.

RESULTS AND DISCUSSION

Seven earth fissures were visually detected using Google Earth (GE) satellite images (Figure 4). Table 2 shows the appearance date and the actual extension of the main fissures according to available information for GE

In accordance with Galloway and Burbey (2011), subsidence caused by groundwater extraction and aquifer compaction is an almost imperceptible phenomenon. The San Joaquin Valley, California, has experienced 9-meter subsidence from 1925 to 1975; well drilling for groundwater use is the principal cause.

Figueroa-Miranda *et al.* (2018) report that Mexico has 99 cities affected by subsidence. Mexico State presents the significant quantities of affected areas, with 17, followed by Jalisco State and Chihuahua State, with 16 and 11, respectively.

The evolution of Earth's fissures is available in the annexes link.

Hydrologic analysis

The weather in the study area indicates that the main precipitation occurs in summer (July, August, and September) with an average annual rainfall of 465.7 mm. Based on meteorological station data and Thiessen polygons, the precipitation regime in the study area over the last few years exhibits a rainfall trend, as illustrated in Figure 5.

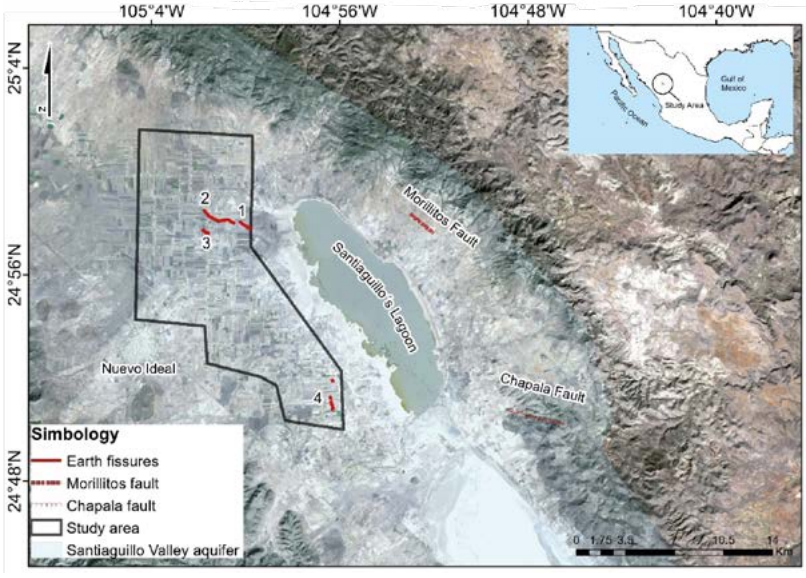

Figure 4. The study area is located inside the Laguna de Santiaguillo watershed, since 2012 is considered a Ramsar Wetland and is cataloged as an Area of Importance for Bird Conservation (AICA).

Table 2. Characteristics of earth fissures.

Fissures	Appearance date	Extension m
1	September 2023	1,002
2	August 2019	2,758
3	September 2019	443
4	January 2021	723

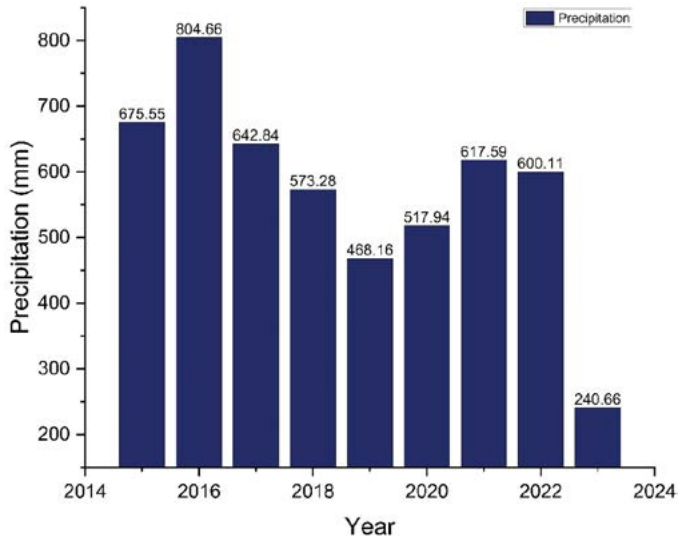

Figure 5. Rainfall volume in the study area over the past 9 years (mm per year).

The aquifer's natural conditions limit the recharge exclusively to precipitation inside the watershed. In the year 2023, rainfall decreased below average, provoking drought conditions in the study area. One of the principal effects of this meteorological phenomenon is the increase in groundwater extraction, which is destined to cover crops' hydraulic needs (Simon Wang *et al.*, 2016).

Due to geological, geophysics, and hydrogeological conditions, Valle de Santiaguillo is defined as a free, heterogeneous, anisotropic aquifer. The upper portion is made of alluvial, fluvial, foothill, lacustrine, and aeolian sediments, as well as polygenic conglomerates (Figure 5), with thicknesses that vary several meters at the center of the valley and gradually decrease towards the vicinity of the mountain range (CONAGUA).

Conditions described by CONAGUA coincide with Zhu *et al.* (2024) definition, which establishes that overexploitation of hydric resources coming from aquifers in compressible alluvial deposits could create subsidence phenomena, which, under specific hydrogeological conditions, are associated with earth fissures. Pacheco-Martínez *et al.* (2013) describe similar geological conditions in Aguascalientes, where earth fissure formation has also occurred.

Groundwater uses

Valle de Santiaguillo aquifer is located inside the endorheic Laguna de Santiaguillo watershed (Figure 6) whose precipitations form runoffs that flow into the lagoon body of the area, and the recharge depends entirely on the rainfalls, CONAGUA, 2020 estimates an annual average recharge of 44.9 hm^3 and 115.13 hm^3 per year are concessioned, based on this information it is evident an aquifer overexploitation condition.

In the study area, according to REPDA, 1,097 registered wells have concessioned a total of 34.08 hm^3 annual volume, with predominance of agricultural concessions in the number of registers. Groundwater concessions located in the study area (16,790 ha)

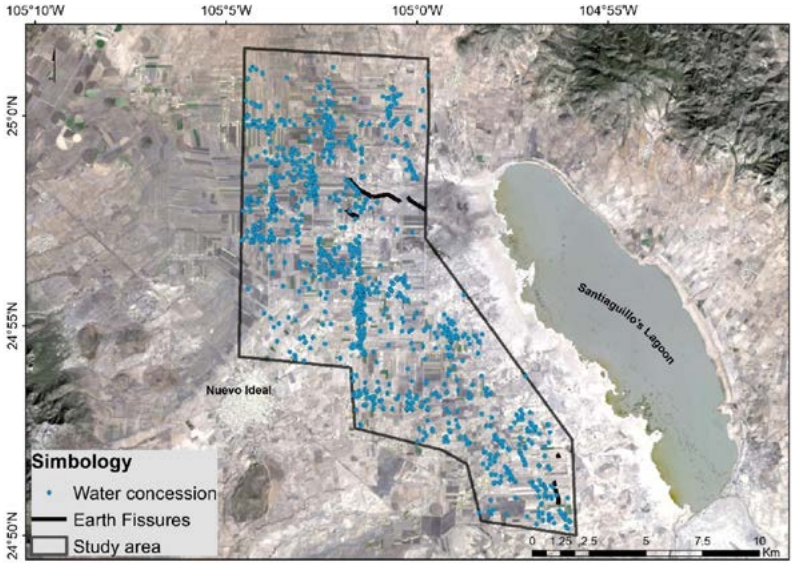

Figure 6. Groundwater concessions within the study area.

represent 30% of the aquifer's (250,400 ha) total volume concessioned, which represents a significant concentration of groundwater extraction in the area.

Kernel density analysis

Number of concessions per Surface unit

Based on REPDA information, the annual concessions volume from the analysis per right was observed to have an average density of 6.46 wells/Km^2, spatially distributed. 82% (138.40 Km^2) of the study area has a low well density with an accumulation from 0-12 wells/Km^2, 15% (25.10 Km^2) has medium density with values from 13-32 wells/Km^2, and 3% (4.40 Km^2) has high density with values from 33-88 wells/Km^2 (Figure 7).

Concessioned volume per surface unit

It was determined that the lowest volumes per square kilometer are in areas where annual concessions range from 0 to 228,654 m^3, corresponding to 70% (117.63 km^2). On the other hand, 24% (40.17 Km^2) of the study area has medium concessions with annual volume values from 228,655 to 705,846 m^3; finally, the areas with higher yearly volume concessions fluctuate from 705,847 to 2'535,084 m^3. Showing that the study area is under intense pressure due to groundwater extractions (Figure 8).

Comparing Kernel density by number of concessions and volume concessioned, it's observed that earth fissures are mainly localized in areas where extraction densities and number of wells are from medium to high. This suggests that pressure exerted on the aquifer in these zones has favored the fissures opening directly related to the location of the concentration of groundwater concessions.

Based on the result analysis, the pressure on the aquifer has encouraged the formation of earth fissures in this area. This phenomenon has already been described by other researchers, who mention that high levels of well drilling, prolonged periods

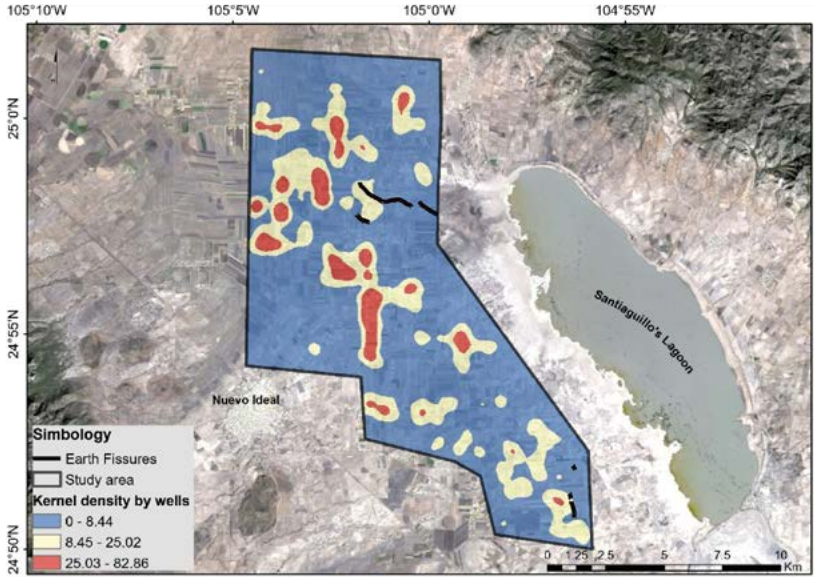

Figure 7. Kernel's density per concession.

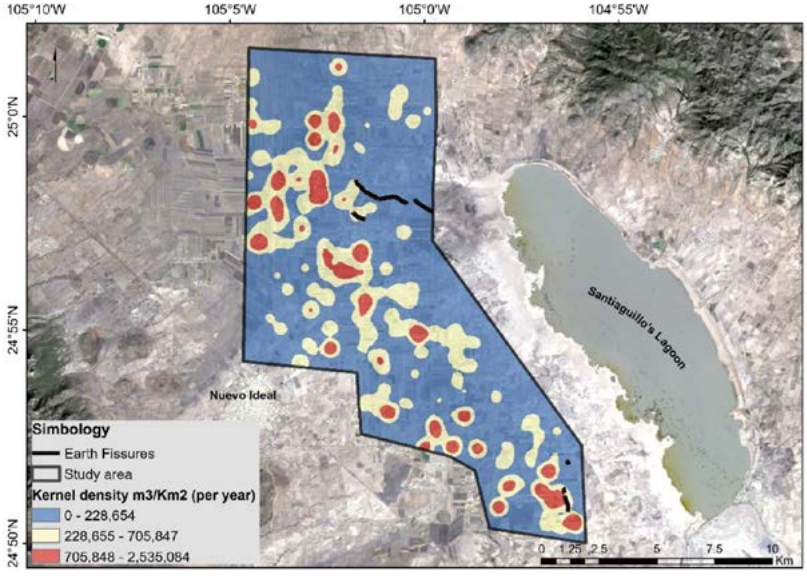

Figure 8. Kernel's density per annual volume concessioned.

of water pumping, an arid or semiarid climate, and a decrease in static levels are factors that facilitate the formation of these failures (Burbey, 2002; Pacheco-Martínez *et al.*, 2013).

Normalized differential moisture index (NDMI)

According to the obtained values for the agriculture cycle 2023, NDMI spatial distribution presents important variations in specific areas during the months of the agriculture cycle; however, it is observed that zones containing major moisture quantities are agricultural production areas, making evident that the moisture patron

is strongly related to agricultural activities in parcels that have groundwater concessions (Figure 9).

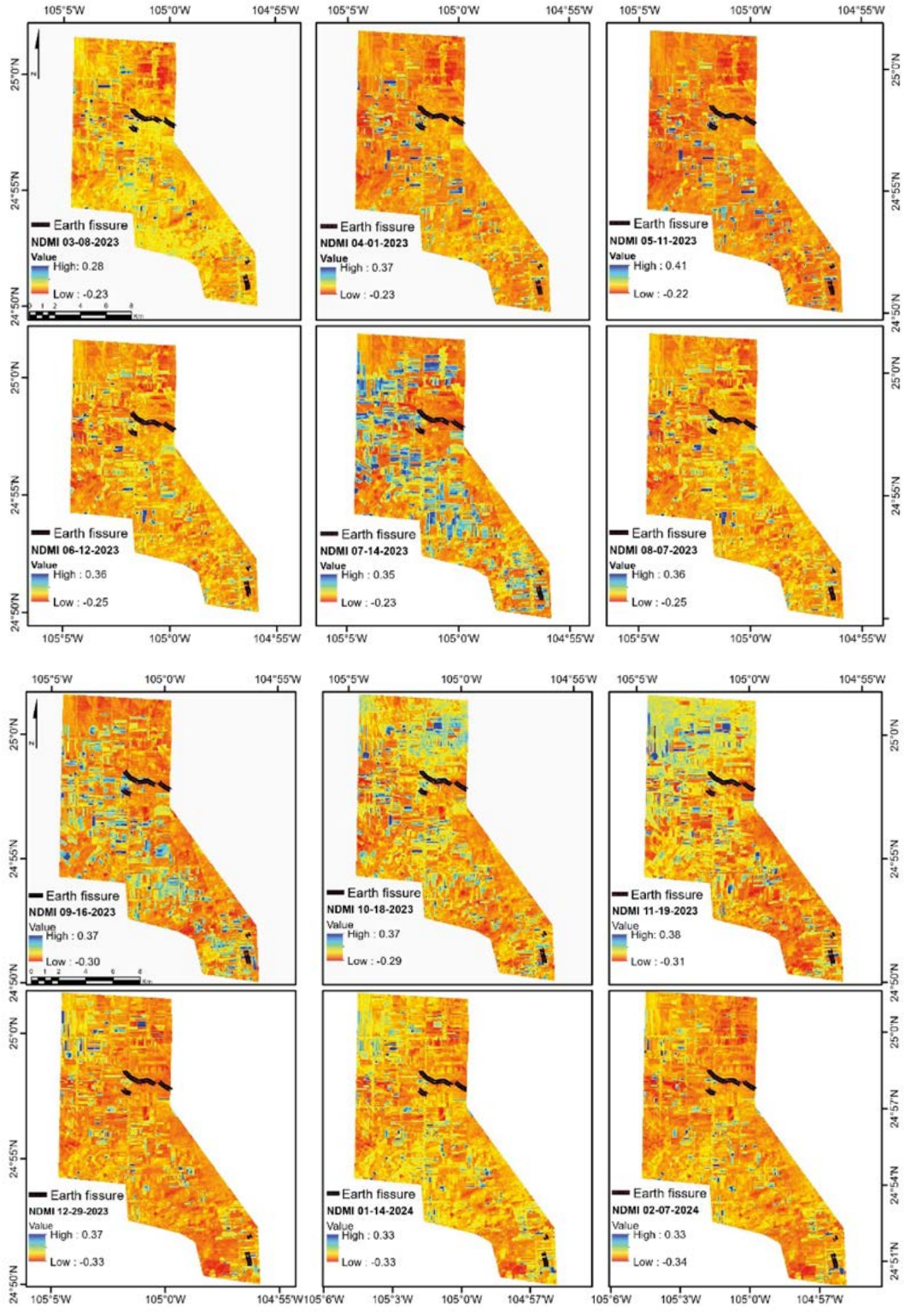

Figure 9. NDMI of the agricultural cycle 2023-2024 in the study area

The average NDMI value for the 2023-2024 agricultural cycle is close to 0, indicating a generalized high hydric stress, with an increase in NDMI value in July, which is attributed to the start of the rainy season in the region (Table 4). However, some parcels present higher moisture levels than others, which is why they have been irrigated even during the rainy season.

The highest NDMI in a parcel (0.41) was observed in May (Table 4), being an abnormal value according to climatological conditions of the region. May is within the drought season, and the main rainfall occurs in the summertime. Thus, the quantity of observed humidity might be related to irrigation activities in parcels

Agricultural activities within the spring-summer cycle, shown in the images (May to September), present a major humidity presence derived from groundwater irrigation. However, winter cycle irrigation activities, although minor, are still present in located parcels with great correspondence, in both cycles, with earth fissure localization, particularly in the south of the study area.

Histograms of NDMI are available in the annexes link.

Comparison analysis between precipitation and NDMI shows a higher humidity level in May and November; this does not coincide with the natural humidity peaks caused by rain.

Sustained hydric stress, evidenced by low average NDMI values, leads to constant groundwater extraction for irrigation, favoring decreasing phreatic levels (van Opstal *et al.*, 2022).

Aquifers overexploitation may lead to land differential subsidence, manifesting throw fissure formation (Alvarez *et al.*, 2001), besides, moistening cycles for irrigation followed by intense evapotranspiration generate ground tensions that aggravate the fracturing, thereby, fissures spatial distribution might be related correlated to, not only to groundwater extraction patterns, but also to superficial humidity captured by NDMI (Zang *et al.*, 2019).

Table 4. Monthly comparison of NDMI of the agricultural cycle 2023-2024.

Date	Maximum	Minimum	Average
03/08/2023	0.28	−0.23	−0.07
04/01/2023	0.36	−0.25	−0.06
05/11/2023	0.41	−0.22	−0.06
06/12/2023	0.35	−0.25	−0.07
07/14/2023	0.35	−0.23	−0.02
08/07/2023	0.35	−0.25	−0.07
09/16/2023	0.37	−0.29	−0.04
10/18/2023	0.37	−0.29	−0.02
11/19/2023	0.38	−0.31	−0.008
12/29/2023	0.37	−0.32	−0.07
01/14/2024	0.33	−0.33	−0.08
02/07/2024	0.33	−0.34	−0.09

According to the analysis of the relation of precipitation and NDMI of 2023 agricultural cycle, maximum NDMI values in dry season (January to May) are comparable to the rainy months (July to September), being evident that anthropogenic activities, especially intensive use groundwater for irrigation, allows to maintain crops humidity levels, even in natural hydric deficit conditions (Figure 10).

Based on the results obtained, it's observed that the study area is subject to strong anthropogenic pressure, and the use of both water and soil resources is evident, as agricultural activities are constantly developed throughout the year. This continuous exploitation not only affects water availability but may also contribute to soil degradation processes, such as earth fissures and subsidence, which are related to decreasing phreatic levels and intensive irrigation management (Faunt *et al.*, 2024).

Based on Tukey test, June and August do not present significant difference in their precipitations, it's also observed that during agricultural cycles there are hydric stress conditions in the study area due to NDMI average is close to 0, from the analyzed period a large amount of aberrant data was obtained that increased the NDMI, and making a comparative it's observed that spatial distribution matches to agricultural parcels that have a groundwater source for irrigation supply (Figure 11).

If the tendency of groundwater extractions in the Laguna de Santiaguillo aquifer continues, the consequences could be similar to those of aquifers on Chile, where research has exposed that a constant exploitation of groundwater might provoke severe effects on hydrological systems, such as disconnection between the aquifer and natural surface water runoff, modifying the aquifer's discharge that supplies wetlands or rivers in the dry season. Finally, excessive groundwater extraction from the aquifer storage rather than natural recharge increases the period required to replenish naturally (Jódar *et al.*, 2024).

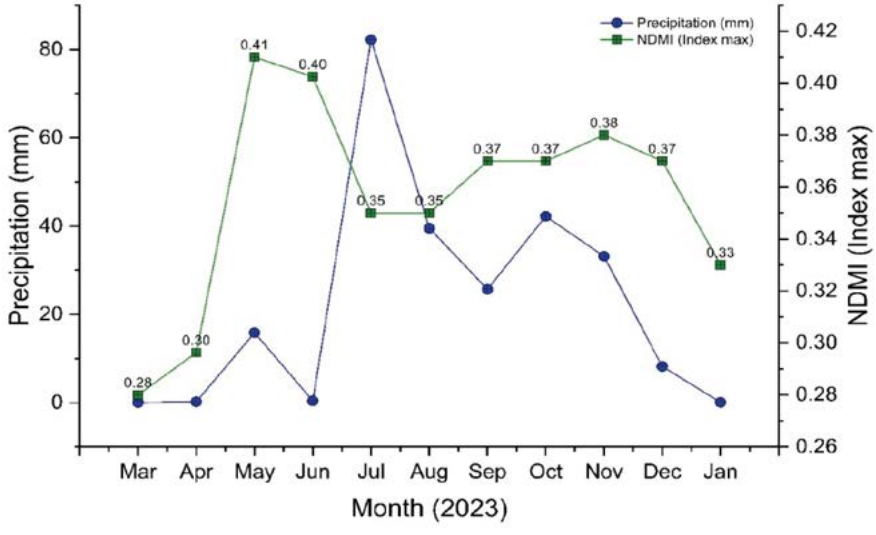

Figure 10. Monthly comparison between NDMI and precipitation

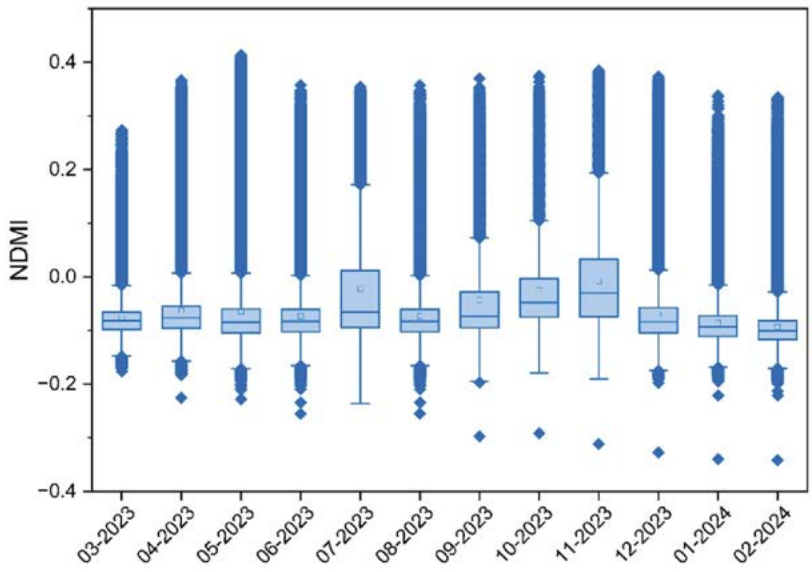

Figure 11. NDMI temporal variation in the spring-summer and autumn-winter agricultural seasons.

CONCLUSIONS

The study area presents significant pressure related to groundwater concessions. According to the Kernel analysis density, it was detected that one of the regions with major volume concessioned density coincides with one of the earth fissures detected through spatial images. These results suggest that this zone presents an advanced subsidence phenomenon.

A constant groundwater extraction throughout the year was detected, as NDMI values surpass monthly natural means, and the areas with major humidity correspond to agricultural parcels that depend on the aquifer. This affects the phreatic levels and may cause a decrease in water volume, pore compression, lower storage capacity, and changes in soil layers.

In 2023, the decrease in rainfall provoked a lower aquifer recharge. This situation, in addition to increasing agricultural groundwater demand, has generated saturation and drying of soil, which in turn has increased the risk of fissure appearance due to the increased efforts on its structure.

The study area's natural characteristics, such as a semiarid climate, the aquifer's lithology characteristics, and the significant groundwater demand destined for agricultural activities, correspond to identified factors in specialized literature that facilitate earth fissure formation.

The location of the longest earth fissure is within a zone that is subject to extensive humidity and drying variations. This condition, in addition to high concession density per square kilometer, can be related to relevant changes in the soil stress state over a considerable area.

ACKNOWLEDGMENT

The authors are grateful for the support provided by CONAHCYT for the doctoral scholarship awarded in the period 2023-2027 with the CVU number 489249, as well as to the National Polytechnic Institute for the BEIFI scholarship.

ANNEXES

https://docs.google.com/document/d/1lWjf4bsSwpR6zUozK_jN2f6meTvdcH9y/edit?usp=drive_link&ouid=113470542075061576459&rtpof=true&sd=true

REFERENCES

Alvarez, A., Garnica, P., Martínez, G.E.I., 2001. Metodologia Para Determinar La Influencia De La Extraccion De Agua Subterranea En La Infraestructura Del Transporte. 1-70.

Barati, A.A., Azadi, H., Scheffran, J., 2019. A system dynamics model of smart groundwater governance. *Agric. Water Manag.* 221, 502-518. https://doi.org/10.1016/j.agwat.2019.03.047

Burbey, T., 2002. The influence of faults in basin-fill deposits on land subsidence, Las Vegas Valley, Nevada, USA. *Hydrogeol. J.* 10, 525-538. https://doi.org/10.1007/s10040-002-0215-7

Chakraborty, A., Basu, P., 2025. Intensive agriculture influences functional diversity, redundancy and trait profile of bee community and interacting plant community in a tropical agricultural landscape. *Agric. Ecosyst. Environ.* 383, 109544. https://doi.org/10.1016/j.agee.2025.109544

CONAGUA, 2020. S Ubdirección G Eneral T Écnica 32.

Dash, S.K., Sembhi, H., Langsdale, M., Wooster, M., Dodd, E., Ghent, D., Sinha, R., 2025. Assessing the field-scale crop water condition over an intensive agricultural plain using UAV-based thermal and multispectral imagery. *J. Hydrol.* 655, 132966. https://doi.org/10.1016/j.jhydrol.2025.132966

Fan, B., Shi, X., Luo, G., Hellwich, O., Ma, X., Shang, M., Wang, Y., Ochege, F.U., 2025. Ground subsidence and disaster risk induced by groundwater overexploitation: A comprehensive assessment from arid oasis regions. *Int. J. Disaster Risk Reduct.* 119, 105328. https://doi.org/10.1016/j.ijdrr.2025.105328

Faunt, C.C., Traum, J.A., Boyce, S.E., Seymour, W.A., Jachens, E.R., Brandt, J.T., Sneed, M., Bond, S., Marcelli, M.F., 2024. Groundwater Sustainability and Land Subsidence in California's Central Valley. *Water* 16, 1189. https://doi.org/10.3390/w16081189

Figueroa-Miranda, S., Tuxpan-Vargas, J., Ramos-Leal, J.A., Hernández-Madrigal, V.M., Villaseñor-Reyes, C.I., 2018. Land subsidence by groundwater over-exploitation from aquifers in tectonic valleys of Central Mexico: A review. *Eng. Geol.* 246, 91-106. https://doi.org/10.1016/j.enggeo.2018.09.023

Galloway, D.L., Burbey, T.J., 2011. Review: Regional land subsidence accompanying groundwater extraction. *Hydrogeol. J.* 19, 1459-1486. https://doi.org/10.1007/s10040-011-0775-5

Jódar, J., Urrutia, J., Herrera, C., Custodio, E., Martos-Rosillo, S., Lambán, L.J., 2024. The catastrophic effects of groundwater intensive exploitation and Megadrought on aquifers in Central Chile: Global change impact projections in water resources based on groundwater balance modeling. *Sci. Total Environ.* 914. https://doi.org/10.1016/j.scitotenv.2023.169651

Pacheco-Martínez, J., Hernandez-Marín, M., Burbey, T.J., González-Cervantes, N., Ortíz-Lozano, J.Á., Zermeño-De-Leon, M.E., Solís-Pinto, A., 2013. Land subsidence and ground failure associated to groundwater exploitation in the Aguascalientes Valley, México. *Eng. Geol.* 164, 172-186. https://doi.org/10.1016/j.enggeo.2013.06.015

Redwan, M., Abdel Moneim, A.A., 2016. Factors controlling groundwater hydrogeochemistry in the area west of Tahta, Sohag, Upper Egypt. *J. African Earth Sci.* 118, 328-338. https://doi.org/10.1016/j.jafrearsci.2015.10.002

SEMARNAT, 2010. El agua en México, Academia Mexicana de Ciencias. Ciudad de México.

Simon Wang, S.-Y., Lin, Y.-H., Gillies, R.R., Hakala, K., 2016. Indications for Protracted Groundwater Depletion after Drought over the Central Valley of California*,+. *J. Hydrometeorol.* 17, 947-955. https://doi.org/10.1175/JHM-D-15-0105.1

Song, M., He, W., An, M., Fang, X., Wang, B., Ramsey, T.S., 2023. Toward better agricultural grey water footprint allocation under economy-resource factors constraint. *Ecol. Indic.* 154, 110806. https://doi.org/10.1016/j.ecolind.2023.110806

Van Camp, M., Radfar, M., Walraevens, K., 2010. Assessment of groundwater storage depletion by overexploitation using simple indicators in an irrigated closed aquifer basin in Iran. *Agric. Water Manag.* 97, 1876-1886. https://doi.org/10.1016/j.agwat.2010.02.006

van Opstal, J.D., Neale, C.M.U., Hipps, L.E., 2022. Evaluating the adaptability of an irrigation district to seasonal water availability using a decade of remotely sensed evapotranspiration estimates. *Agric. Water Manag.* 261, 107383. https://doi.org/10.1016/j.agwat.2021.107383

Whittemore, D.O., Butler, J.J., Bohling, G.C., Wilson, B.B., 2023. Are we saving water? Simple methods for assessing the effectiveness of groundwater conservation measures. *Agric. Water Manag.* 287, 108408. https://doi.org/10.1016/j.agwat.2023.108408

Yan, Y., Shi, H., Miao, Q., Zhao, Y., Nie, X., Li, Z., Pan, M., Feng, W., Gonçalves, J.M., Duarte, I.M., 2025. Evolution of chemical characteristics and irrigation suitability of groundwater in arid and semi-arid regions. *Agric. Water Manag*. 311, 109361. https://doi.org/10.1016/j.agwat.2025.109361

Zang, M., Peng, J., Qi, S., 2019. Earth fissures developed within collapsible loess area caused by groundwater uplift in Weihe watershed, northwestern China. *J. Asian Earth Sci*. 173, 364-373. https://doi.org/10.1016/j.jseaes.2019.01.034

Zhu, L., Li, J., Gong, H., Ye, M., Dai, Z., Li, X., Teatini, P., 2024. Simulating earth deformation evolution caused by groundwater pumping through ordinary state-based Peridynamics method. *J. Hydrol*. 634, 131133. https://doi.org/10.1016/j.jhydrol.2024.131133